scientific reports

Check for updates

OPEN

Dysregulated landscape of RNA-binding proteins in unexplained recurrent spontaneous abortion revealed by bulk and single-cell transcriptome

Yaqi Zhu[1], Dongjuan Chen[1], Bingbing Xu[2], Xiaoxue Wu[1], Ao Liang[1] & Qiuyue Yan[1]✉

In recurrent spontaneous abortion (RSA), impaired decidualization due to decidual stromal cell (DS) apoptosis or pyroptosis disrupts pregnancy maintenance. RNA-binding proteins (RBPs) are crucial regulators of gene expression in reproductive disorders. However, the comprehensive profile and dynamic role of RBPs in DS cells during RSA are not fully understood. In this study, single-cell transcriptome sequencing (scRNA-seq) data originated from six decidua tissues of RSA group and five health controls were downloaded and analyzed by differentially expressed genes (DEGs) analysis, pseudotime analysis, functional enrichment analysis, RBPs regulatory program analysis, transcription factor regulatory network analysis, correlation analysis and etc. We employed bulk RNA-seq data (including three RSA decidua tissues and three decidua in normal early pregnancy) to confirm the results from scRNA-seq data. DS cells were the most abundant population in decidua and the primary dysregulated type in RSA, showing a reduced proportion. DS harbored the most DEGs, enriched in post-transcriptional regulation. RBPs served as effective markers for cell annotation and reflected pathological states. Decorin (DCN) and lectin galactoside-binding soluble 3 (LGALS3) were upregulated, while ribosomal protein S17 (RPS17) was downregulated across various cells. The DS subclusters RBP-DS_0, 2, and 4 were diminished in RSA, with RBP-DS_2 nearly absent. Pseudotime analysis revealed an aberrant DS differentiation trajectory from State1 (pseudotime starting point) to State2 linked to abnormal progression in RSA. The expression of DCN, LGALS3, and solute carrier family 3 member 2 (SLC3A2) in DS subpopulations was significantly elevated in RSA and peaked in State2 along the pseudotime. This study explores RBPs for cell annotation and clustering in decidual tissue. Our findings implicated the regulatory role of RBPs in RSA pathogenesis and highlighted three key RBPs (DCN, LGALS3, and SLC3A2) whose upregulation in DS subclusters during the progression of RSA may be associated with aberrant differentiation, suggesting their potential as biomarkers and therapeutic targets.

Keywords Recurrent spontaneous abortion, Decidual stromal cells, Single-cell RNA sequencing analysis, Bulk RNA sequencing analysis, RNA-binding proteins

Recurrent spontaneous abortion (RSA), also termed recurrent pregnancy loss (RPL) or recurrent miscarriage[1], constitutes a highly heterogeneous disorder clinically defined as two or more recognized pregnancy failures, affecting approximately 2.5% of women attempting conception. While miscarriage diagnosis is relatively straightforward, advancements in predicting and preventing RSA are constrained by the absence of standardized definitions, uncertainties in pathogenesis and substantial variability in clinical manifestations[2]. During human placentation, the uterus undergoes a series of transformations. Initially, the endometrial stromal compartment differentiates into decidua. Subsequently, fetal-derived placental villous trophoblasts (PVTs) traverse the uterine epithelium and invade both the decidua and the inner third of the myometrium. Finally, trophoblast differentiates,

[1]Department of Laboratory Medicine, Maternal and Child Health Hospital of Hubei Province, Tongji Medical College, Huazhong University of Science and Technology, Wuhan 430070, People's Republic Of China. [2]Department of Sports Medicine, Peking University Third Hospital, Institute of Sports Medicine of Peking University, Beijing 100191, People's Republic Of China. ✉email: yanqiuyue2014@163.com

which is characterized by the invasion of extravillous trophoblasts (EVTs) into the uterine spiral arteries and the extensive remodeling of these vessels[3]. The etiology of RSA is complex and multifactorial, potentially involving genetic predisposition, anatomical abnormalities, endocrine disorders, and immunological factors. However, approximately 50% of clinical RSA cases remain idiopathic, classified as "unexplained recurrent pregnancy loss", highlighting the current limitations in our understanding of its pathogenesis[4]. Therefore, in-depth research into the pathological mechanisms of RSA is particularly crucial for its effective treatment and management.

The differentiation of hESCs plays a pivotal role in sustaining pregnancy. During the establishment and maintenance of gestation, hESCs undergo dynamic transformation which involves a precisely regulated balance among cellular proliferation, differentiation, and apoptosis. However, in patients with recurrent pregnancy loss, DS exhibit excessive apoptosis or over pyroptosis, resulting in decidualization defects that impair pregnancy maintenance[5,6]. The maternal immune cells are recruited via chemokine gradients produced by DS and trophoblast[7]. The maintenance of immune homeostasis at the maternal-fetal interface is particularly critical for successful pregnancy establishment and sustenance. Pathological alterations in the endometrial immune microenvironment are associated with severe reproductive disorders, including recurrent implantation failure (RIF) and unexplained RSA[8].

RNA-binding proteins (RBPs) serve as pivotal effectors of gene expression[9], and their abnormal expression is the basis of many diseases[10,11]. RBPs play an important role in female reproductive pathologies, particularly in inflammatory processes and immune dysregulation-mediated pathological mechanisms[12,13]. It has been demonstrated that the abnormal elevation of IGF2BP3 in the pregnant endometrium leads to the impairment of decidualization and abnormal trophoblast invasion, thereby predisposing individuals to RSA[14]. However, there are few studies on the expression profiles of RBPs in different cells types (including both immune and non-immune cells) and the abnormal regulation related to RSA.

In this study, we performed a comprehensive identification and annotation of cell populations for RSA tissues through scRNA-seq analysis. We analyzed differentially expressed RBPs (DE-RBPs) in different cell types and compared the relative proportion changes of RBP-defined clusters. Our analysis placed particular emphasis on DS cells and determined their RBP-based clustering. Pseudotime analysis was employed to identify key DS subpopulations and delineate the differentiation trajectory associated with the progression of RSA. By integrating bulk RNA-seq data from decidual tissues and performing overlap analysis, we revealed the core RBPs (DCN, LGALS3 and SLC3A2) related to RSA pathogenesis. Our study suggested the distinctive characteristics and aberrant expression patterns of RBPs in different cell types, especially in DS from RSA. These findings advance our understanding of their potential regulatory roles in RSA progression, as well as proposed novel targets for RSA diagnostic biomarkers and therapeutic intervention.

Materials and methods

Retrieval and process of public data

To explore the potential functions and the expression pattern across various cellular types of RBPs, we analyzed the scRNA-seq dataset from 5 healthy controls and 6 RSA decidual tissues (PRJNA672658, Supplemental Table S1) with unexplained reason[15], and integrated the bulk RNA-seq from 3 RSA and 3 healthy controls (PRJNA819201)[16]. Samples of the RSA group were collected from women with RSA after the diagnosis of missed abortion. Decidua was identified and washed in phosphate-buffered saline and used for the single cell isolation and following experiments. Fastq.gz files of scRNA-seq data of RSA and Health samples were downloaded from PRJNA672658 (https://www.ncbi.nlm.nih.gov/bioproject/PRJNA672658). The CellRanger (version 7.0.0) pipeline (https://www.10xgenomics.com/support/software/cell-ranger/latest) was utilized to generate a digital gene expression matrix. The UMI count matrix was converted into a Seurat object by the R package Seurat[17](version 4.3.0). Cells with UMI numbers < 1000 or detected genes < 500 or over 15% mitochondrial-derived UMI counts were considered low-quality cells and were removed, ultimately retaining 73,628 cells. Genes detected in less than 5 cells were removed for the downstream analyses.

Fastq.gz files of bulk RNA-seq data of unexplained recurrent spontaneous abortion (URSA) samples and normally early pregnancy (NEP) control were downloaded from PRJNA819201 (https://www.ncbi.nlm.nih.gov/bioproject/PRJNA819201). Raw reads were aligned to the GRCh38 genome by HISAT2[18]. Uniquely mapped reads were used for gene reads number counting and FPKM calculation (fragments per kilobase of transcript per million fragments mapped)[19].

ScRNA-seq data preprocessing

After quality control, matrixes from different samples were merged by Seurat for cross-sample comparison in the following analysis. Particularly, the merged count matrixes were log-normalized by 'Normalize Data' function and scaled by 'Scale Data' function. Then, the 2000 most variable genes were identified by 'Find Variable Features' function and principal components (PCs) were calculated by 'Run PCA' function. Then we conducted data integration through the harmony algorithm[20]. Nearest neighbors were computed based on the top 30 PCs, and then clusters were identified by 'Find Clusters' function (resolution = 0.4). And then they were visualized with tSNE or UMAP plots. To identify the cell type for each cluster, we detected gene markers for each cell clusters using the 'Wilcoxauc' function in Presto (version 1.0.0) package, then we annotated cell types using ScType tools[21].

DEGs analysis

ScRNA-seq: DEGs were determined with the 'Wilcoxauc' function from the Presto package. For computing DEGs, all genes were probed that the expression difference on a natural log scale was at least 0.5 and the difference of percent of detected cells was at least 0.2 and adjusted p-value was less than 0.05.

Bulk RNA-seq: The R Bioconductor package DESeq2 (v.1.18.3)[22] was adopted to screen out the DEGs. The qvalue ≤ 0.05 and fold change ≥ 2 were set as the cut-off criteria for identifying DEGs.

Pseudotime analysis

Monocle 2 was used for pseudotime analysis, trajectory construction and calculation of pseudotime-dependent gene expression (Monocle 2[23], version 2.26.0). DDRTree (version 0.1.5) method is used for dimension reduction. Cell trajectory was visualized according to cell subtypes and cell states. The Basic Differential Analysis algorithm is used to identify DEGs according to pseudotime function. BEAM (Branched Expression Analysis Modeling) was used to identify genes that are regulated in a branching-dependent manner.

Functional enrichment analysis

To sort out functional categories of genes, Gene Ontology (GO) terms and Kyoto Encyclopedia of Genes and Genomes (KEGG) pathways were identified using KOBAS 2.0[24]. Hypergeometric test and Benjamini-Hochberg FDR controlling procedure were applied to define the enrichment of each pathway.

RBPs regulatory program analysis

The UMI count matrix of 2,141 RBPs[25] were extracted as input for Seurat of cell cluster. Differentially activated RBPs were selected using 'Wilcoxauc' function from the Presto package.

Correlation analysis

After we have set up our Seurat object, the first step is to construct metacells from the single-cell dataset[15]. Briefly, metacells are aggregates of small groups composed of similar cells derived from the same biological sample of origin. The k-Nearest Neighbors (KNN) algorithm was used to identify groups of similar cells to aggregate. Then the average or summed expression of these cells was computed, thus yielding a metacell gene expression matrix. The sparsity of the metacell expression matrix was considerably reduced when compared to the original expression matrix. Therefore, it is preferable to use. We calculated the Pearson's correlation coefficient between genes used the corr.test function that comes with the R package, and filter |correlation| ≥ 0.9, p-value < 0.01.

Transcription factor regulatory network analysis

The modules of TFs were identified by the SCENIC[26] python workflow (version 0.11.2) using default parameters (http://scenic.aertslab.org). A human TF gene list was used from the resources of pySCENIC (https://github.com/aertslab/pySCENIC/tree/master/resources). Activated TFs were identified in the AUC matrix and differentially activated TFs were selected using R package limma[27]. To identify cluster-specific regulons (especially for analyses with many cell types, where some regulons are common to multiple of them) we used the Regulon Specificity Score (RSS)[28]. Networks of the modules with TFs and their target genes were visualized by Cytoscape (v.3.9.1) (https://cytoscape.org/).

Other statistical analysis

The stat_compare_means in ggpubr R package (https://rpkgs.datanovia.com/ggpubr/) was used for comparisons between two groups (Student's t-test).

Results

ScRNA-seq analysis of the RSA-deregulated functions in different cell types of decidua

The etiology of RSA is complex and multifactorial, potentially involving genetic predisposition, anatomical abnormalities, endocrine disorders, and immunological factor. The proliferation and invasion of EVTs, DS proliferation with subsequent decidualization, and immunological homeostasis are particularly critical for establishing as well as maintaining pregnancy. To elucidate the key regulatory factors influencing RSA progression, we used both scRNA-seq and bulk RNA-seq datasets and integrated the analysis results to identify the regulatory RBPs that potentially affect RSA pathogenesis or progression (Fig. 1A). For scRNA-seq, we identified 11 major cell populations (Fig. 1B), including Dendritic cells (DC), DS, fibroblasts (FB), NK, macrophages (Macro), T cells, plasma cells (Plasma), perivascular cells (PV), endothelial cells (Endo), EVT, and epithelial cells (Epi), with DS representing the predominant cell type. Each cellular subset exhibited distinct high expression patterns of representative genes and RBPs (Fig. 1C-D). Each cell cluster also represented a signature expression pattern based on its marker genes (Supplementary Fig. 1A). Analysis of cellular proportions in different tissue samples from the RSA and Health groups revealed that the predominant cell populations consisted of DS, Macro cells, and NK cells. A notable finding was that the proportion of DS was reduced in the RSA group, while an increase in FB cell population was observed (Fig. 1E). GO enrichment analysis of the differentially expressed genes (DEGs) revealed that upregulated genes in the RSA group were significantly enriched in pathways such as mitogen activated protein kinase (MAPK) signaling, insulin-like growth factor (IGF) signaling, Wnt signaling, innate immune response, and hormonal stimulus response. Conversely, downregulated genes primarily demonstrated enrichment in hypoxia response and cellular respiration pathways (Fig. 1F). Transcriptomic analysis of DEGs between the RSA and healthy groups demonstrated that DS exhibited the highest number of DEGs, followed by FB cells (Fig. 1G). Subsequently, GO pathway enrichment analyses were performed on DEGs in multiple cell types. In DS, upregulated DEGs exhibited significant enrichment in pathways which are associated with post-transcriptional regulation, including IGF signaling, Wnt signaling, cell adhesion, antigen presentation, positive regulation of T cell-mediated cytotoxicity, cytoplasmic translation and transcriptional regulation by RNA polymerase II (Fig. 1H). Conversely, downregulated DEGs were predominantly enriched in pathways associated with hypoxia response, mitochondrial electron transport and transport-related processes, cellular translation and ribosomal subunit assembly (Fig. 1I). Enrichment analysis of DEGs in DS within post-

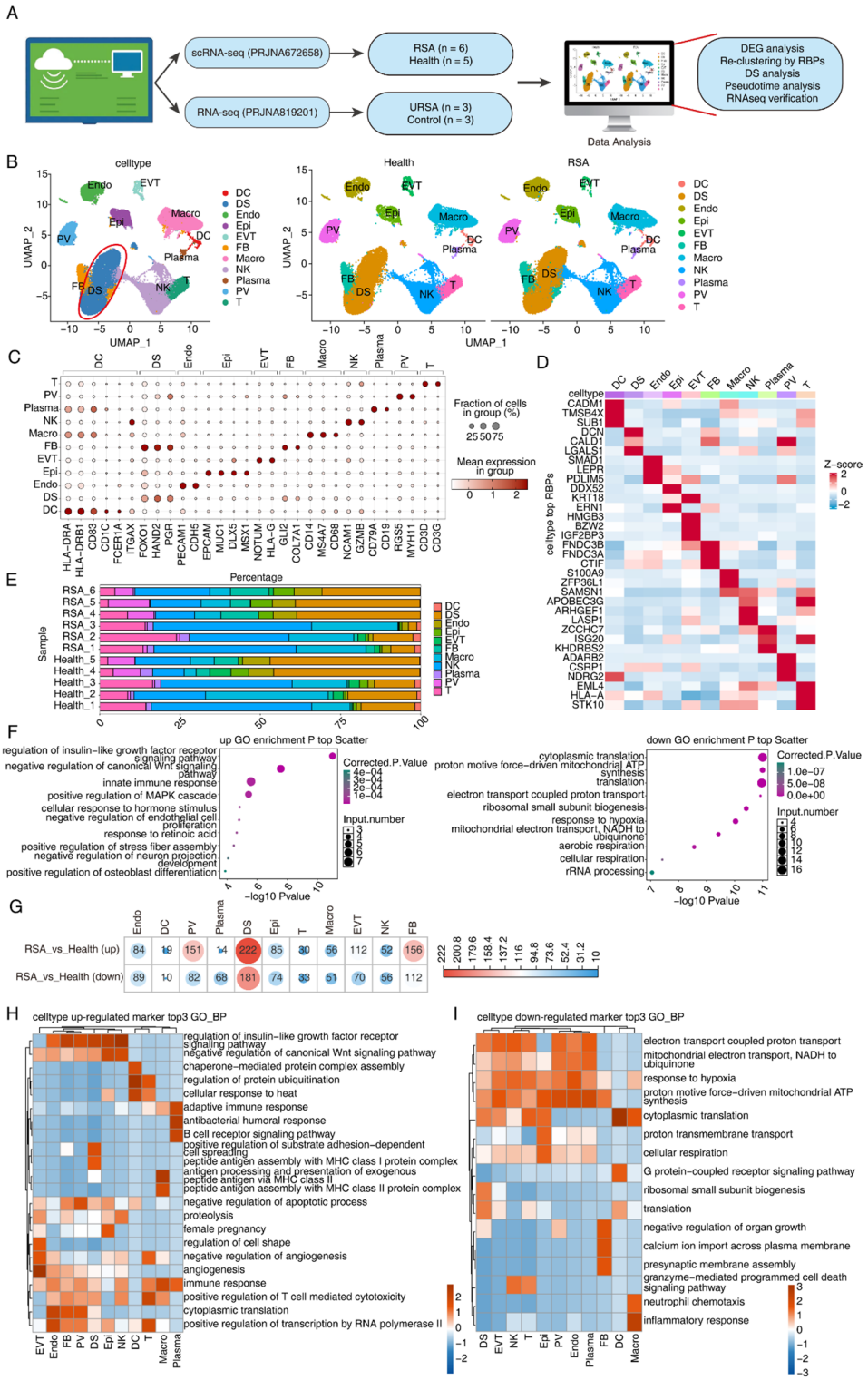

transcriptional regulatory pathways suggests the potential involvement of RBP-mediated dysregulation of target genes during the pathological progression of RSA. Therefore, RBPs show cell-type specificity comparable to that of established marker genes. These RBPs molecular signatures could not only serve as useful identifiers for cellular classification but also are implicated in maintaining cell-specific functions within defined physiological contexts. The heatmaps of gene enrichment analysis illustrated the enrichment patterns of different cell types in various biological processes (GO) and signaling pathways (KEGG). Specifically, Supplementary Fig. 1B and C showed the combined marker enrichment across cell types in GO and KEGG pathways respectively, while Supplementary Fig. 1D and E focused on the enrichment of up-regulated and down-regulated markers in KEGG pathways for each cell type.

◀**Fig. 1**. ScRNA-seq analysis of the RSA-deregulated functions in different cell types of decidua. (**A**) Working flow of this study showing the salient features of this study. (**B**) UMAP plot of single-cell transcriptomic profiles from RSA and Health samples based on highly variable genes. Colors indicate cell annotations. (**C**) Dot plot shows expression of representative genes in each cell type. (**D**) Heatmap shows the average expression of top3 RBP genes in each cell type. (**E**) Stacked bar chart comparing the proportions of cell populations of each cell type within each sample group. (**F**) Bar plot Bubble Chart shows top10 GO biological process enrichment pathways obtained by up-regulated genes or down-regulated genes between RSA group compared to the Heath group in all cell type. (**G**) Dot plot shows the statistical results of the number of DEGs in each cell type. (**H**) The heatmap shows top3 GO biological process enrichment pathways obtained by up-regulated genes between RSA group compared to the Heath group in each cell type. (**I**) The heatmap shows top3 GO biological process enrichment pathways obtained by down-regulated genes between RSA group compared to the Heath group in each cell type.

ScRNA-seq analysis of RBP expression identifies cell type-specific RBP clusters in RSA and healthy decidua

To investigate whether the expression of RBPs exhibits distinctive features that can be used for cell annotation, we performed unsupervised clustering by Seurat based on the expression levels of 2,141 previously reported RBPs genes[25,29]. This analysis yielded 15 RBP-clusters (R0-R14), which exhibited cell clustering patterns largely consistent with those identified by marker genes. These clusters were subsequently annotated into 11 cell types (Fig. 2A, B). RBP-clusters also displayed high expression of specific characteristic RBPs (Fig. 2C), which were potentially involved in cell identification and contributed to cellular functions in specific environments. By analyzing the composition structure of RBP-clusters in different cell types, we found that for most cell types, the expression pattern of RBPs has strong cell-type specificity (with 1–2 dominant RBP-clusters characterizing each population), For instance, DS are predominantly composed of the R0-cluster, Endo cells primarily consist of R7 and R11-cluster, and FB cells are mainly characterized by the R4-cluster (Fig. 2D). A reduction in the proportion of R0-cluster in DS alongside an increased representation of FB-like R4-cluster was observed in RSA patients relative to healthy controls. Subsequently, we analyzed the expression changes of selected characteristic RBPs between the Health and RSA groups. DCN exhibited the most pronounced upregulation in R0 and R8-clusters of DS-like cells. CUGBP Elav-like family member 2 (CELF2) demonstrated high expression levels in the R1, R2, R5, and R10 clusters. However, when comparing the Health and RSA groups overall, its expression showed only minimal alterations. Significant increases in CELF2 expression were specifically observed in the R0 and R8 clusters. These findings suggested that DCN and CELF2 may regulate target gene expression in DS cells, possibly influencing the progression of RSA. RNA binding motif protein 47 (RBM47) and Quaking (QKI) primarily exhibited an increase within the R5-cluster (Fig. 2E). They may modulate immune responses through the regulation of antigen presentation in DC cells, indicating their possible involvement in the pathogenesis of RSA. Our single-cell analysis of RSA revealed no statistically significant differences in insulin-like growth factor 2 mRNA binding protein 3 (IGF2BP3) and zinc finger protein 36 (ZFP36) expression among various cell types (Supplementary Fig. 2A). Finally, we conducted GO/KEGG pathway enrichment analyses on the top RBP genes within RBP-clusters (Fig. 2F), illustrating the functional roles of RBPs in post-transcriptional regulation on gene expression. In summary, RBPs not only serve as reliable markers for cellular annotation but also demonstrated a correlation with the state of pathological alterations.

ScRNA-seq analysis of RSA-deregulated RBPs in various cell types of decidua

To explore the regulatory role of RBPs in cellular processes, we categorized cell types into immune cells (including DC, NK, T, Plasma and Macro cells) and non-immune cells (comprising FB, PV, EVT, DS, Epi, and Endo cells). The RBPs were further classified into upregulated and downregulated groups. Subsequently, we performed overlap analysis of RBPs that exhibited concurrent upregulation or downregulation in both immune and non-immune cell populations (Fig. 3A). In immune cells, DCN presents upregulated expression across four immune cell types, while LGALS3, major histocompatibility complex, class I, A (HLA-A), and heat shock protein family A member 1 A (HSPA1A) show elevated expression in three immune cell subsets. Conversely, RPS17 demonstrates downregulated expression in four immune cell types, as well as ribosomal protein L31 (RPL31) is suppressed in three immune cell populations. Among non-immune cells, LGALS3 and DCN display upregulated expression in six cell types, whereas vimentin (VIM), ribosomal protein L18 (RPL18), jun proto-oncogene (JUN), and ribosomal protein L13 (RPL13) exhibit increased expression in five cell types. Poly(A) binding protein cytoplasmic 4 (PABPC4), RPS17 and ribosomal protein L17 (RPL17) exhibited downregulated expression in four cell types. The consistent upregulation of DCN and LGALS3 across multiple immune and non-immune cell lineages, coupled with the widespread downregulation of RPS17 in diverse cell populations, implies their potential functional significance in RSA. We conducted GO/KEGG functional enrichment analysis on upregulated and downregulated RBP genes across different cell types. The results revealed that RBPs were enriched not only in post-transcriptional regulatory pathways but also in other functional pathways. For instance, EVT-upregulated RBPs showed enrichment in the PI3K/Akt positive regulation pathway, Epi-upregulated RBPs were enriched in the apoptotic positive regulation pathway, DS-upregulated RBPs exhibited enrichment in the peptide antigen assembly pathway of MHC class I protein complexes, and Endo-upregulated RBPs were enriched in innate immune responses. Conversely, Endo-upregulated RBPs were enriched in transforming growth factor-β (TGF-β) and Hippo signaling pathways, while FB-downregulated RBPs were enriched in ECM-receptor interaction and PPAR signaling pathways (Fig. 3B-C). Functional enrichment analysis of GO/KEGG pathways for both upregulated and downregulated RBP genes in RBP-clusters exhibited characteristics consistent with

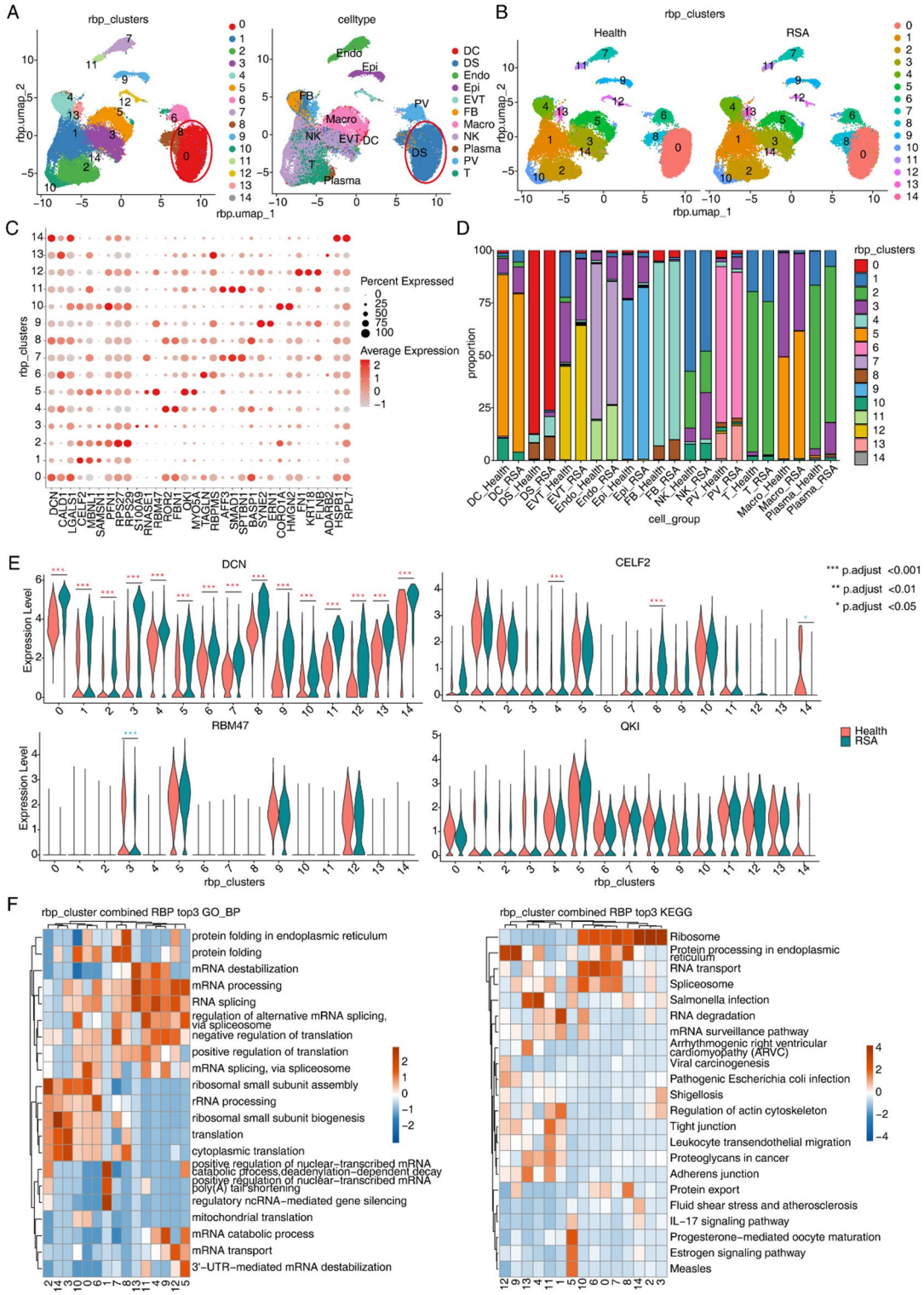

Fig. 2. ScRNA-seq analysis of RBP expression identifies cell type-specific RBP clusters in RSA and healthy decidua. (**A**) UMAP plot of single-cell transcriptomic profiles from RSA and Health samples based on RBP genes. Colors indicate RBP clusters. (**B**) UMAP plot of RSA and Health groups single-cell transcriptomic profiles based on RBP genes. Colors indicate RBP clusters. (**C**) The dot plot shows expression of top3 RBP genes in each RBP cluster. (**D**) Stacked bar chart displays the percentage of different RBP cluster in different cell type. (**E**) The violin plot displays the expression of the selected genes in different RBP cluster. (**F**) The heatmap shows top3 GO biological process or KEGG enrichment pathways obtained by marker genes in each RBP cluster.

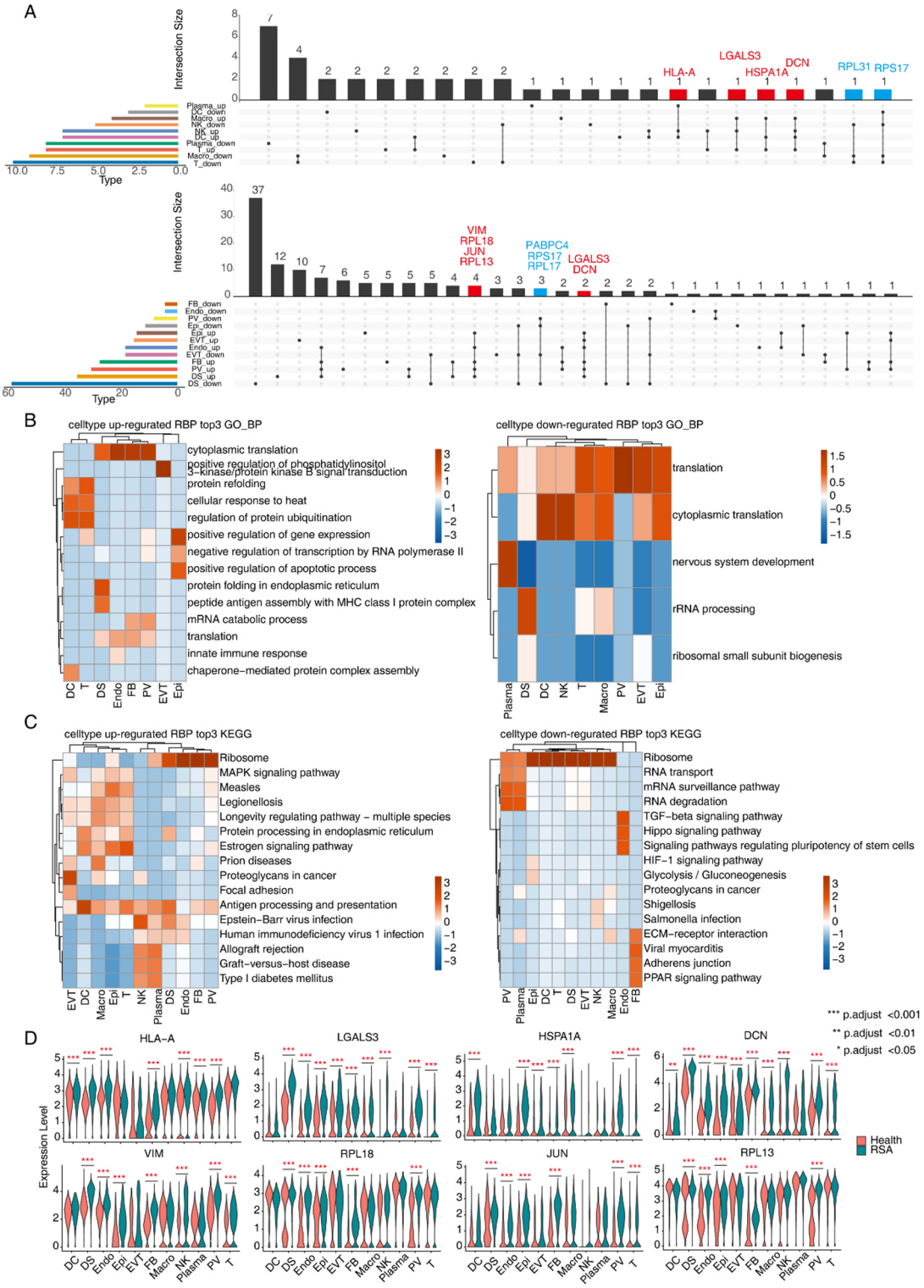

Fig. 3. ScRNA-seq analysis of RSA-deregulated RBPs in various cell types of decidua. (**A**) Upset diagram shows the number of overlapped DE-RBPs in different cell types. Top: Upregulated and downregulated RBPs among immune cell types; Bottom: Upregulated and downregulated RBPs across non-immune cell types. Genes marked in red represent upregulation, while those in blue indicate downregulation. (**B**) The heatmap shows top3 GO biological process enrichment pathways obtained by up-regulated (left) and down-regulated (right) RBP genes in different cell types. (**C**) The heatmap shows top3 KEGG pathways obtained by up-regulated (left) and down-regulated (right) RBP genes in different cell types. (**D**) The violin plot displays the expression of the selected up-regulated RBP genes in different cell types.

those observed in individual cell types (Supplementary Fig. 3A, B). Our analysis of differentially expressed RBPs in multiple cell types presented in Fig. 3A revealed distinct expression patterns. As demonstrated in Fig. 3D, the RSA group exhibited significant upregulation of DCN and LGALS3 expression in DS, Endo, Epi, EVT, FB, Macro, Plasma, NK, PV and T cells compared to the healthy control. Conversely, RPS17 showed marked downregulation in DS, Endo, Epi, FB, Macro and PV cells. Several additional RBPs, such as HLA-A, HSPA1A, VIM, RPL18, JUN, and RPL13, displayed distinct expression patterns marked by selective up-regulation in diverse immune and non-immune cell populations (Fig. 3D), while RPL31, RPS17, PABPC4 and PRL17 were selectively down-regulated (Supplementary Fig. 3C). These findings point to that RSA is not an isolated issue of individual cells, but rather involves systemic alterations of the holistic microenvironment involving multiple cell types. The coordinated upregulation and downregulation of RBPs could establish a molecular state that is incompatible with normal pregnancy.

ScRNA-seq analysis of RSA-deregulated RBPs in different cell subtypes of DS cells

Given that DS constitute the most abundant cell population in decidual tissues and serve as a key component during the decidualization process, we conducted independent clustering analyses and found that DS can be categorized into six distinct subpopulations (DS_0–5) (Fig. 4A, B). Moreover, each DS cluster exhibited distinct overexpression patterns of characteristic marker genes and RBPs (Fig. 4C-D), suggesting that RBPs possess cell-type specificity similar to that of marker genes within DS. The result of cellular subpopulation distribution among different sample groups indicated that DS were predominantly composed of DS_0 and DS_1 subtypes. Analysis of the RSA group showed increased proportions of DS_0 and DS_2, while a decreased proportion was observed for DS_1 (Fig. 4E). Our analysis revealed that the RBP-annotated DS clusters (designated as RBP-DS-clusters) exhibited distinct cell-type specificity, enabling the classification of DS into five distinct subpopulations (RBP-DS_0–4) (Fig. 4F-G). We further depicted the proportion of different subtype of DS cell RBP cluster in different subtype of DS cells and the percentage of different subtype of DS in different subtype of DS cell RBP cluster (Supplementary Fig. 4A). Distribution analysis showed that the primary clusters for RBP-DS_0 to RBP-DS_4 were as follows: DS_0 and DS_1 for RBP-DS_0, DS_3 for RBP-DS_1, DS_0 for RBP-DS_2, DS_2 and DS_5 for RBP-DS_3, and DS_4 for RBP-DS_4. Each RBP-DS-cluster demonstrated unique expression profiles of RBP genes (Fig. 4H). We further analyzed the cellular proportions of RBP-DS-clusters in different samples, revealing that RBP-DS_0, 1, and 2 constituted the predominant cellular populations. Compared with the Health group, the RSA group exhibited significant increase in RBP-DS_1 and 3, accompanied by a reduction in RBP-DS_0, 2 and 4. Notably, RBP-DS_2 was nearly eliminated in the RSA group (Fig. 4I). The diminished cellular subpopulations may represent aberrant subsets associated with RSA pathogenesis. Differential expression analysis was performed on the genes from these increased and decreased RBP-DS-clusters, followed by GO/KEGG enrichment analyses (Supplementary Fig. 4B, C). For RBP-DS_0, the upregulated genes were mainly enriched in angiogenesis, ATP production, oxidative phosphorylation, cellular protein synthesis, and protein folding, while the downregulated genes were significantly enriched in negative regulation of cell growth, TGF-β signaling, ECM-receptor interaction, Rap1 signaling, and Hippo signaling. In RBP-DS_2, the upregulated genes were largely involved in angiogenesis, extracellular matrix buildup and mitochondrial respiratory function, whereas the downregulated genes were enriched in pathways related to cellular response to hypoxia, integrated stress response and apoptosis that are tightly associated with the pathogenesis of RSA[30,31]. These findings identified new cell subpopulations within DS and observed their proportional changes in RSA. These subpopulations may be participated in maintaining normal pregnancy and are related to the development of RSA.

Single cell pseudotime analysis revealed differentiation dynamics and key RBPs in DS cells with RSA

To delineate the differentiation trajectory of DS, we performed pseudotime analysis on representative DS and determined three well-defined cell states (State 1–3). State 1 mainly localized at the pseudotemporal origin (Fig. 5A). DS_1 subpopulation primarily distributed in State 1, DS_0 in State 2, and DS_2 in State 3. Subsequent analysis of RBP-DS-clusters in relation to pseudotime revealed that State 1 and State 2 branches were predominantly composed of RBP-DS_0, while State 3 largely comprised RBP-DS_1. RSA group exhibited an increase in cell clusters in State 2 and a reduction in the proportion of cells in State 3 (Fig. 5B and Supplementary Fig. 5A). The co-localization of DS_0 and RBP-DS_0 in State2 indicated their similarity and relevance to RSA progression. The temporal dynamics of cellular density for each State changing with pseudotime were illustrated in Fig. 5C. State1 represents the early pseudotime phase, corresponding to the normal pre-differentiation cellular state. State2 and State3 reside in the late pseudotime phase, suggestive of the differentiated cellular state associated with RSA progression. Notably, when DS cells differentiate to the branch point 1, their developmental trajectories begin to diverge, bifurcating into two different differentiation states.

To investigate the pseudotime-differential RBPs conceivably responsible for trajectory anomalies, we applied BEAM analysis at branch point 1, revealing two distinct cell fates. Fate 1 maps to the direction of State 2 and fate 2 aligns with State 3. These differential expression of RBPs could be clustered into three functional modules (cluster 1–3) over pseudotime. The RBPs in module 1 primarily are linked to fate 2, while module 3 mostly are implicated in fate 1 determination. The RBPs in module 2 are positioned at the anterior branch of cell fate determination and may function during the transitional phase (Fig. 5D). We then compared the proportions of cell populations of each state within each sample group (Fig. 5E) and each sample (Supplementary Fig. 5B). The result indicated a significant increase in the proportion of cells in State 2 and a concomitant decrease in State 1 cell populations in the RSA group relative to the health control. The differentiation trajectory of State 2 may be associated with aberrant progression in gestational decidualization in RSA. We further focused on the specific RBPs that are involved in cell fate over pseudotime (Fig. 5F). Muscleblind-like protein 1 (MNBL1) in module 1 is associated with fate 2, exhibiting an overall upregulation trend along the pseudotime. However, its expression

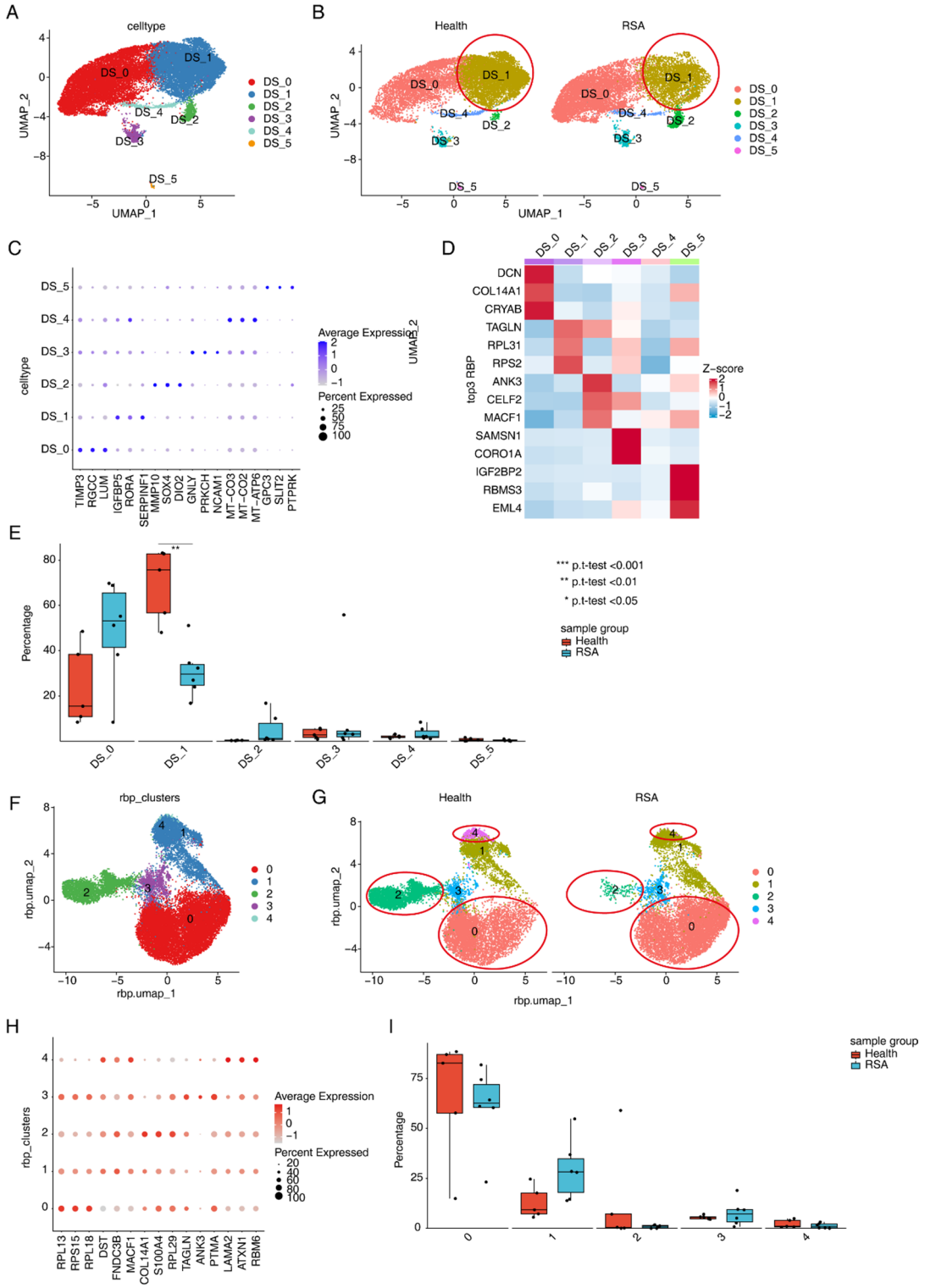

Fig. 4. ScRNA-seq analysis of RSA-deregulated RBPs in different subclusters of DS cells. (**A**) UMAP plot of single-cell transcriptomic profiles from DS based on highly variable genes. Colors indicate subtype of DS cell clusters. (**B**) UMAP plot of RSA and Health groups single-cell transcriptomic profiles based on highly variable genes. Colors indicate DS cell clusters. (**C**) Dot plot shows expression of top3 marker genes in each subtype of DS cell type. (**D**) Heatmap shows the average expression of top3 RBP genes in each subtype of DS cell type. (**E**) Bar plot comparing the proportions of cell populations of each subtype of DS cell type within each sample group. (**F**) UMAP plot of single-cell transcriptomic profiles from DS based on RBP genes. Colors indicate subtype of DS cell RBP clusters. (**G**) UMAP plot of RSA and Health groups single-cell transcriptomic profiles based on RBP genes. Colors indicate DS cell RBP clusters. (**H**) The dot plot shows expression of top3 RBP genes in each subtype of DS cell RBP cluster. (**I**) Bar plot comparing the proportions of cell populations of each DS cell RBP cluster within each sample group.

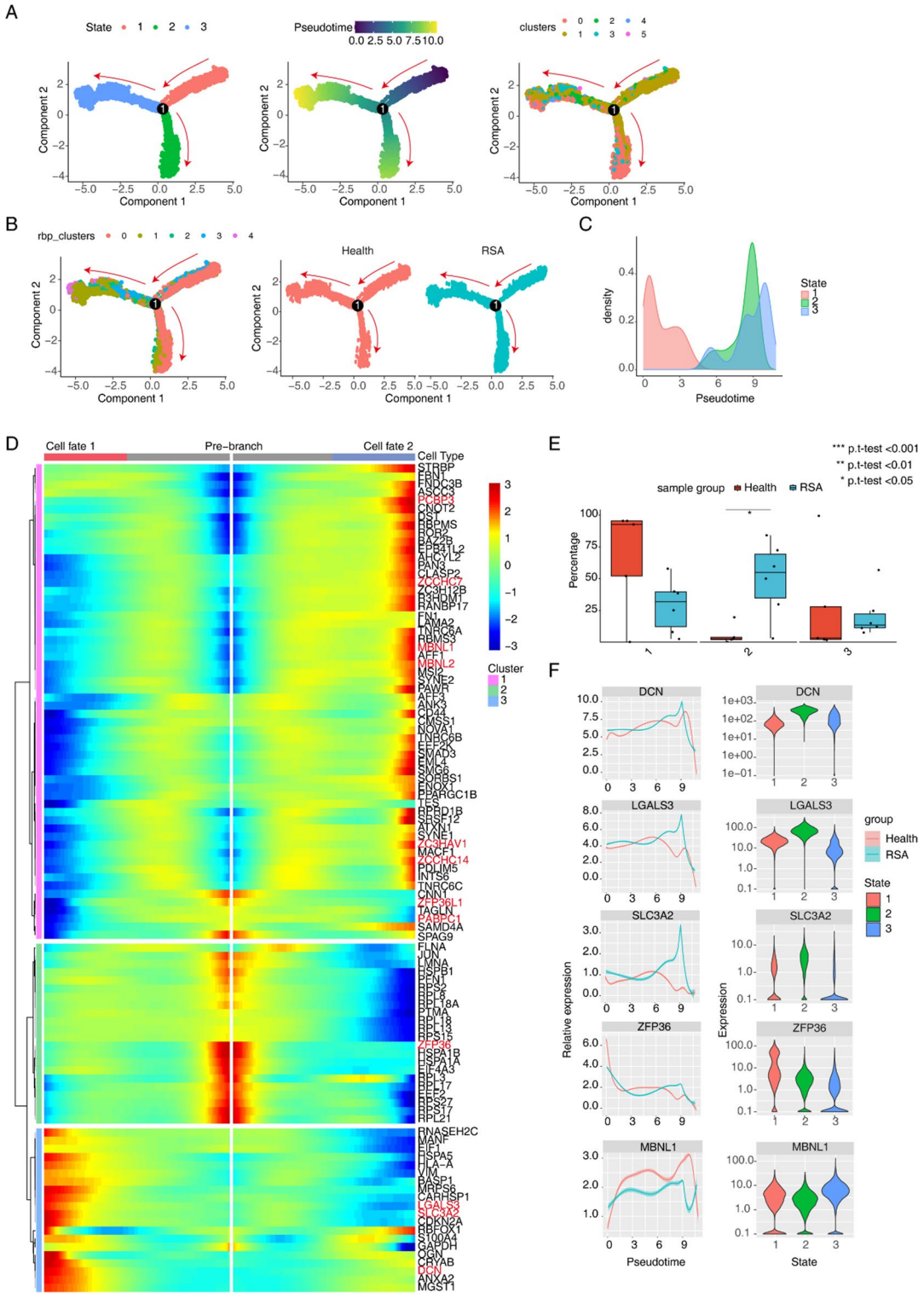

Fig. 5. Single cell pseudotime analysis revealed differentiation dynamics and key RBPs in DS cells with RSA. (**A**) UMAP plots of pseudotime analysis for DS subpopulations. DS are colored by state, cluster and their progression through pseudotime. (**B**) DS are colored by subtype of DS cell rbp cluster and groups through pseudotime. (**C**) Density plot of each state changing with pseudotime. (**D**) The beam_heatmap using BEAM analysis showing the changes in two lineages at the time point 1, the columns of the heatmap are the points in the pseudotime and the rows are the genes. (**E**) Bar plot comparing the proportions of cell populations of each state within each sample group. (**F**) The graph showing the expression of genes in different state and the expression trend of genes over time in each group.

level in the health group is higher than that in the RSA group, reaching the peak in state 3. ZFP36 in module 2 is linked to the anterior branch of cell fate determination, showing a gradual downregulation over pseudotime, with the highest expression observed in state 1 and decreased levels in States 2 and 3. DCN, LGALS3, and SLC3A2 within module 3 exhibit an upward expression pattern correlating with fate 1 over pseudotime and reach the peak expression levels in State 2.

Through the cell annotation and proportion analysis of RBPs, it was observed that the proportions of RBP-DS_0, 2 and 4 were reduced in RSA (Fig. 4I). The observed reduction in the proportion of DS is mainly due to a decrease in these specific subpopulations. This reduction may represent a contributing factor in the pathological progression of RSA. By overlapping differentially expressed RBPs (DE-RBPs) from RBP-DS_0, 2 and 4 with the top 100 RBPs, we obtained the overlapping DE-RBPs (olpDE-RBPs) associated with RSA progression (Supplementary Fig. 5C). DCN and SLC3A2 were upregulated in RBP-DS_0, while LGALS3 was upregulated in both RBP-DS_0 and RBP-DS_2. Conversely, DCN expression was decreased in RBP-DS_2. These results highlight the key DS subpopulations involved in RSA pathology and identify the core RBPs (DCN, LGALS3 and SLC3A2) linked to RSA that are related to cell fate decisions.

Bulk RNA-seq data confirmed the key RSA-deregulated RBPs uncovered by scRNA-seq

To corroborate the discovery of RBPs in scRNA-seq data, we collected bulk-RNA seq data from decidual tissues of three RSA patients and three normal pregnant women. We performed an overlap analysis between differentially upregulated and downregulated RBPs identified in bulk RNA-seq and DE-RBPs obtained from scRNA-seq, yielding 14 co-upregulated differentially expressed RBPs (coDE-RBPs) with no co-downregulated counterparts (Fig. 6A). We then focused on DCN, LGALS3, SLC3A2 and ZFP36 (Fig. 6B). DCN, LGALS3, and SLC3A2 exhibited upregulated expression in both bulk RNA-seq and the RBP-DS_0 subpopulation, whereas DCN showed downregulation in the RBP-DS_2 subpopulation. This implies that DCN may exerts different functions within distinct DS subpopulations. ZFP36 demonstrated downregulation in RBP-DS 0 but was upregulated in both RBP-DS_2 and bulk RNA-seq. IGF2BP3 displayed no significant differential expression in DS subpopulations but was markedly downregulated in bulk RNA-seq. Fig. 6C demonstrated that DCN, LGALS3, SLC3A2 and ZFP36 were significantly up-regulated in URSA group compared to the Control. In summary, our analysis of the bulk RNA-seq data corroborated a set of recurrently dysregulated RBPs (including DCN, LGALS3, and SLC3A2) connected to the pathological progression of RSA.

Discussion

According to guidelines developed by the European Society of Human Reproduction and Embryology (ESHRE) and the American Society for Reproductive Medicine (ASRM), RPL is defined as the failure of two or more pregnancies that are clinically recognized[32,33]. A number of risk factors have been linked to recurrent pregnancy loss, such as structural uterine abnormalities and autoimmune disorders[2]. Data derived from preclinical animal models have indicated that an impaired decidual response result in pregnancy loss[5,34,35]. It has been hypothesized that the evolution of spontaneous decidualization in humans gives rise to human-specific disorders of pregnancy, including miscarriage and RPL[36]. In this study, scRNA-seq dataset was used to uncover RBP-defined decidual stromal cell subpopulation imbalance in RSA, with abnormal differentiation trajectory. Core RBP genes (DCN, LGALS3, SLC3A2) were identified to be upregulated in RSA, which serve as potential diagnostic biomarkers and therapeutic targets for RSA (Fig. 7).

We employed RBPs to annotate and cluster cells in decidual tissue for the first time. Each cell subpopulation distinctly exhibits high expression of specific marker genes and RBPs. This indicates that RBPs exhibit cell specificity analogous to that of characteristic marker genes, suggesting their potential utility for the identification of cell identity and the maintenance of cell function under specific environmental conditions. We confirmed that DS represent the most abundant cell type within the decidua tissues, which is consistent with previous report[15]. We also discovered that DS cells exhibited the highest number of DEGs, implying that dysregulation of decidualization related gene expression plays an important role in RSA pathogenesis. Analysis showed that DEGs in DS cells were mainly involved in post-transcriptional regulatory pathways, supporting the possibility that DS cells may harbor extensive dysregulation of RBPs in mediating target gene expressions during the pathogenesis of RSA. Patients diagnosed with RSA exhibited marked abnormalities in decidualization and significant disruptions in intercellular communication between stromal cells and other cell types[15]. Current literature primarily employs conventional gene markers for the annotation and typing of DS cells[37], whereas the utilization of RBPs for DS cells annotation has not been extensively explored. In our study, we identified heterogeneous DS cells annotated by RBPs in human decidua, with each stromal subset displaying its own unique features. The proportions of DS cells, along with their subpopulations, including DS_1 and RBP-DS_0, 2 and 4 were significantly lower in the RSA group. In patients with RSA, apoptosis or excessive pyroptosis of DS cells leads to impaired decidualization, which affects pregnancy maintenance. This decreased cell subpopulation could be a major contributing factor to the apoptosis of DS cells. This finding signifies that stromal cells may be unable to furnish sufficient support for fetal development and is closely linked to the development of RSA. During the onset of RSA, it is plausible that stromal cells exhibit defective decidualization, which further leads to alterations to the cellular composition within the decidual microenvironment. Pseudotime analysis revealed that DS predominantly differentiate towards the State2 in the context of RSA. DS_0 and RBP-DS_0 are mainly distributed in State2, indicating both subpopulations share cellular similarities and are associated with RSA progression.

RBPs interact with RNA to form ribonucleoprotein (RNP) complexes that regulate the maturation and fate of target RNA substrates and regulate many aspects of gene expression[10,25]. Previous studies have highlighted the importance of RBPs and their contributions to reproductive pathologies, noting their significant role in female reproductive disorders, particularly in pathological processes mediated by inflammatory and immune

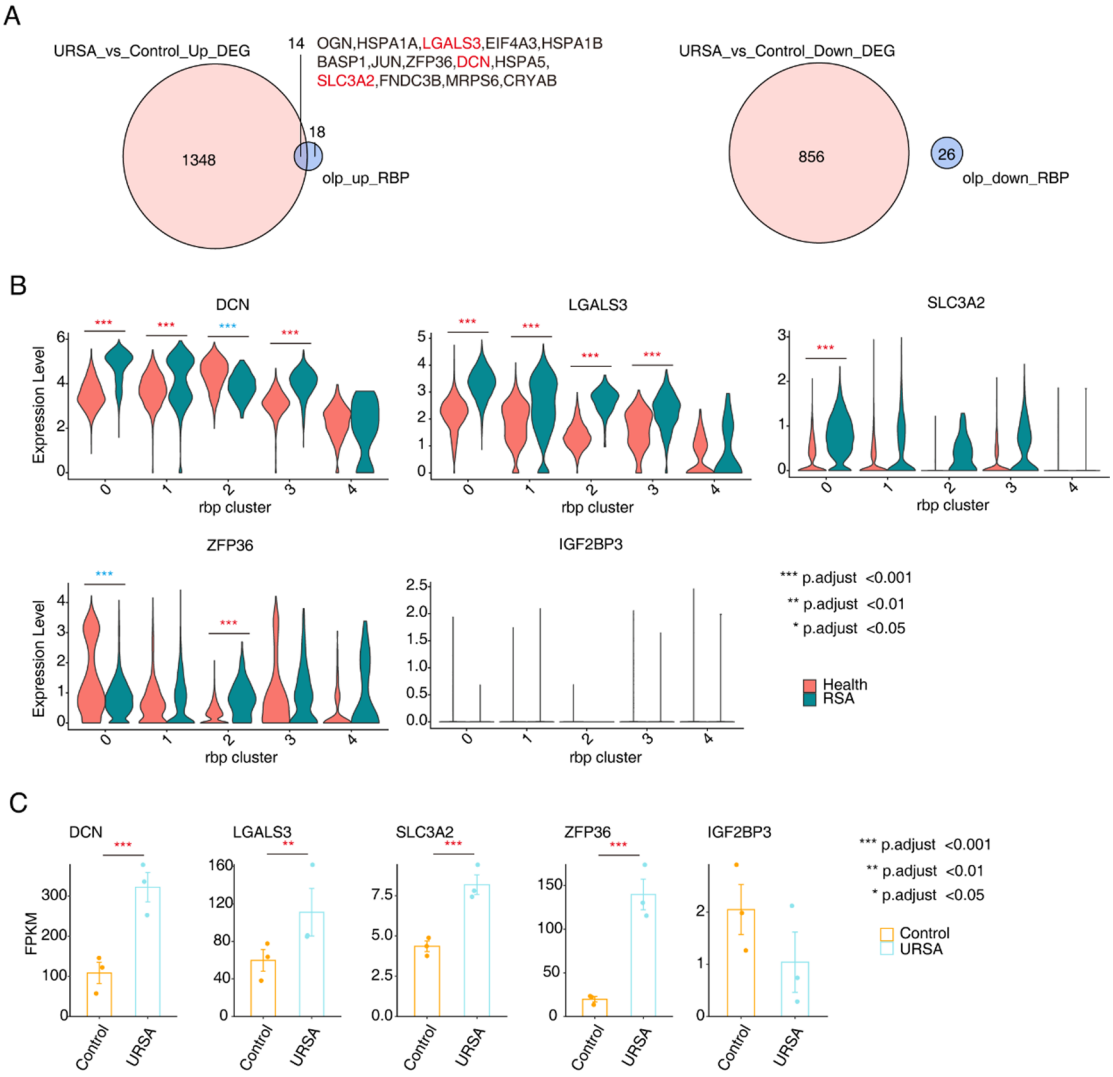

Fig. 6. Bulk RNA-seq data confirmed the key RSA-deregulated RBPs uncovered by scRNA-seq. (**A**) Venn diagram shows the number of overlapped up-regulated (left) or down-regulated (right) genes between the overlapped RBP genes from Supplementary Fig. 5C and DEGs from bulk RNA-seq. (**B**)The violin plot displays the expression of the selected genes in different DS cell RBP cluster. (**C**) The Bar plot displays the expression of selected genes in bulk RNA-seq.

dysregulation[12,38]. The present study characterizes the RBPs genes related to RSA and profile the unique RBPs expression signatures as well as regulatory patterns in different cell types, especially in DS cells at the single-cell level within RSA patients and healthy individuals. Aberrations in DCN levels are correlated with various adverse pregnancy outcomes, encompassing preeclampsia, fetal growth restriction, and preterm premature rupture of membranes[39,40]. DCN promotes decidual M1-like macrophage polarization via mitochondrial dysfunction resulting in RSA[39]. In this study, we found that high levels of DS-derived DCN were detected in the decidua of women in RSA group, consistent with conclusions reported in the existing literature[15]. Galectin-3 (Gal-3), the protein product of the LGALS3 gene, possesses anti-apoptotic activity[41] and displays different functions contingent on its intracellular and extracellular localization[42]. Both LGALS3 and Gal-3 have been consistently identified as participants in the pathogenesis of various diseases, such as prostate cancer, cardiovascular disease, acute and chronic kidney injury, multiple solid tumors, organ fibrosis, and autoimmune inflammatory diseases[43,44]. Gal-3 is a galactose-binding protein; furthermore, it acts as a contributing factor in a broad spectrum of pregnancy related pathologies. Specifically, it is reported that Gal-3 is associated with gestational diabetes mellitus, trophoblast cell function/placentation, pre-eclampsia, intrauterine growth restriction and missed abortions[45]. Gal-3 is markedly decreased in serum, decidua and the villi in the group of women with missed abortions[44]. However, the expression level and potential role of LGALS3 in RSA have not been well investigated. Our findings indicate that LGALS3 gene exhibits distinctly upregulated expression in the RSA group. This phenomenon could potentially be explained if highly expressed LGALS3 activates macrophages and stimulates their secretion of proinflammatory/profibrotic factors, inducing chronic decidual inflammation and basement membrane thickening, which consequently could restrict embryonic implantation and placental

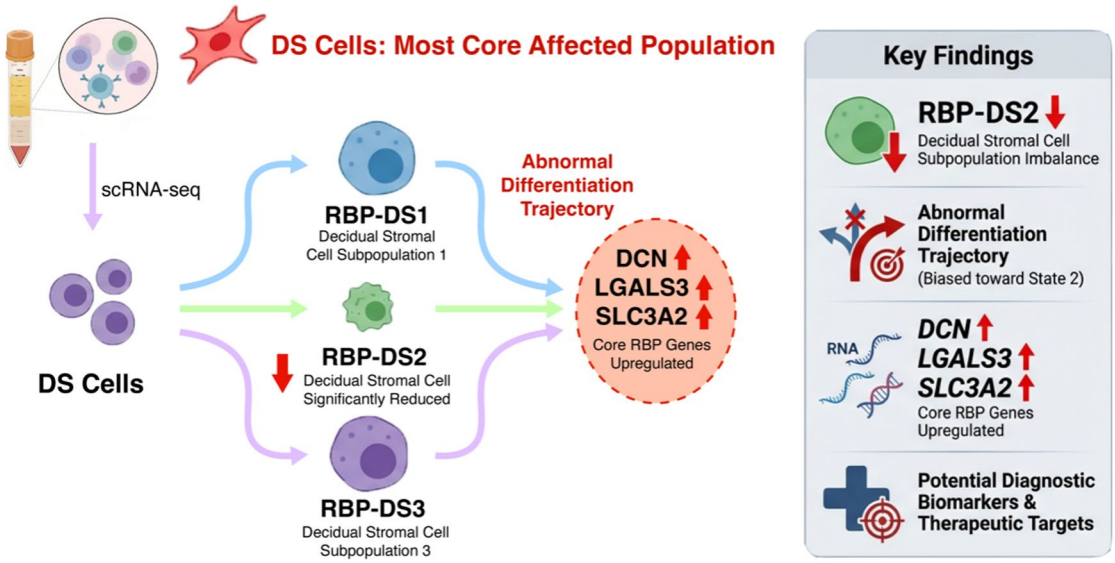

Fig. 7. The summary figure showing the essential results and discoveries of this study.

development. SLC3A2 is a type of transmembrane glycoprotein[46], which usually acts as a chaperone, functions in the cell membrane[47]. A study revealed that TNF superfamily member 14-positive (TNFSF14+) decidual NK cells modulate the senescence homeostasis of DS cells through the TNFRSF14-SLC3A2/leucine regulatory axis, thus facilitating the establishment and maintenance of normal pregnancy. Dysregulation of this axis may induce excessive senescence of DS cells, consequently increasing the risk of spontaneous abortion[48]. Our analysis also indicated higher SLC3A2 expression in DS cells from patients with RSA compared to those from normal pregnancy. DCN and SLC3A2 have been consistently reported as upregulated genes and linked to RSA[39,48]. Nevertheless, their expression profiles across different cell types based on marker gene, as well as RBP annotations within decidual tissues remain insufficiently characterized. This study focuses on RBP clusters within DS cells in order to address this gap.

We found that DCN, LGALS3, and SLC3A2 exhibited upregulated expression in both bulk RNA-seq and the RBP-DS_0 subpopulation, whereas DCN showed downregulation in the RBP-DS_2 subpopulation, suggesting its potential divergent roles among distinct DS subpopulations. ZFP36 and IGF2BP3, as two previously studied RBPs, have been reported to exhibit downregulated expression in murine RSA models[49,50]. However, our single-cell analysis of RSA revealed no statistically significant differences in their expression among various cell types. ZFP36 demonstrated downregulation in RBP-DS_0 but upregulation in both RBP-DS_2 and bulk RNA-seq, a finding inconsistent with its downregulated expression in RSA mouse models, which highlights the value of investigating the pathological impact of RBPs at the human level in RSA[46]. IGF2BP3 expression is downregulated in villous tissues of both RSA patients and murine RSA models. This downregulation contributes to RSA pathogenesis by promoting glutathione peroxidase 4 (GPX4)-mediated ferroptosis while inhibiting trophoblast invasion and migration[50]. We observed that IGF2BP3 exhibits no statistically significant differential expression in the DS subpopulations, yet demonstrates marked downregulation in bulk RNA-seq analysis. This observation aligns with prior research in RSA murine models[51], suggesting that it may not play a major role in modulating RSA progression within DS cells.

The findings of this study need to be viewed in light of some limitations. First, although we applied rigorous batch correction, technical confounders from integrating public datasets might still influence the clustering and differential expression results. Second, the definition of cell clusters and their annotations, while based on established markers, remains interpretative and would benefit from validation through spatial transcriptomics or proteomic approaches. Most importantly, as a purely bioinformatic investigation, our findings are associative and hypothesis-generating. A key limitation is the absence of experimental validation for our central findings, including how these identified RBPs are regulated in decidual cells. While our scRNA-seq outcomes are complemented by supportive evidence from bulk RNA-seq data, this does not constitute functional proof. Consequently, future work must prioritize experimental validation on cell or animal models of these candidate RBPs to definitively elucidate their roles in the signaling mechanisms underlying RSA. This work thus provides a foundational bedrock, defining a clear set of targets and a roadmap for future experimental studies to move from correlation to causation in understanding RSA.

Conclusion

In conclusion, our findings demonstrated the utility of RBPs for annotating and clustering distinct cell subsets. We characterized the distinct features and dysregulated expression of RBPs in different decidual cell types, with a particular focus on DS cells in RSA. Building on this, we then inferred the regulatory functions and potential signaling pathways governed by RBPs during RSA progression. Notably, we identified the key RBPs (DCN, LGALS3 and SLC3A2) in DS subpopulation that are associated with the aberrant decidualization process of

RSA. Integrated analysis of scRNA-seq and bulk RNA-seq data provides insights into the complex regulatory networks controlled by RBPs in the pathological development of RSA. Our findings offer novel perspectives on the factors mediating RSA progression, as well as may inform future strategies for the diagnosis and advanced intervention of RSA.

Data availability

The data that support the findings of this study are available in the supplementary file of this article. Further inquiries can be directed to the corresponding author.

Received: 26 October 2025; Accepted: 16 March 2026
Published online: 01 April 2026

References

1. RPL, E. G. G. et al. ESHRE guideline: recurrent pregnancy loss: an update in 2022. *Hum Reprod Open* hoad002, (2023). https://doi.org/10.1093/hropen/hoad002 (2023).
2. Dimitriadis, E., Menkhorst, E., Saito, S., Kutteh, W. H. & Brosens, J. J. Recurrent pregnancy loss. *Nat. Rev. Dis. Primers.* **6**, 98. https://doi.org/10.1038/s41572-020-00228-z (2020).
3. PrabhuDas, M. et al. Immune mechanisms at the maternal-fetal interface: perspectives and challenges. *Nat. Immunol.* **16**, 328–334. https://doi.org/10.1038/ni.3131 (2015).
4. Papas, R. S. & Kutteh, W. H. A new algorithm for the evaluation of recurrent pregnancy loss redefining unexplained miscarriage: review of current guidelines. *Curr. Opin. Obstet. Gynecol.* **32**, 371–379. https://doi.org/10.1097/GCO.0000000000000647 (2020).
5. Cha, J., Sun, X. & Dey, S. K. Mechanisms of implantation: strategies for successful pregnancy. *Nat. Med.* **18**, 1754–1767. https://doi.org/10.1038/nm.3012 (2012).
6. Liang, Y. et al. JAZF1 safeguards human endometrial stromal cells survival and decidualization by repressing the transcription of G0S2. *Commun. Biol.* **6**, 568. https://doi.org/10.1038/s42003-023-04931-x (2023).
7. Ander, S. E., Diamond, M. S. & Coyne, C. B. Immune responses at the maternal-fetal interface. *Sci. Immunol.* **4** https://doi.org/10.1126/sciimmunol.aat6114 (2019).
8. Li, D., Zheng, L., Zhao, D., Xu, Y. & Wang, Y. The Role of Immune Cells in Recurrent Spontaneous Abortion. *Reprod. Sci.* **28**, 3303–3315. https://doi.org/10.1007/s43032-021-00599-y (2021).
9. Glisovic, T., Bachorik, J. L., Yong, J. & Dreyfuss, G. RNA-binding proteins and post-transcriptional gene regulation. *FEBS Lett.* **582**, 1977–1986. https://doi.org/10.1016/j.febslet.2008.03.004 (2008).
10. Gebauer, F., Schwarzl, T., Valcarcel, J. & Hentze, M. W. RNA-binding proteins in human genetic disease. *Nat. Rev. Genet.* **22**, 185–198. https://doi.org/10.1038/s41576-020-00302-y (2021).
11. Lukong, K. E., Chang, K. W., Khandjian, E. W. & Richard, S. RNA-binding proteins in human genetic disease. *Trends Genet.* **24**, 416–425. https://doi.org/10.1016/j.tig.2008.05.004 (2008).
12. Khalaj, K. et al. RNA-Binding Proteins in Female Reproductive Pathologies. *Am. J. Pathol.* **187**, 1200–1210. https://doi.org/10.1016/j.ajpath.2017.01.017 (2017).
13. Van Nostrand, E. L. et al. A large-scale binding and functional map of human RNA-binding proteins. *Nature* **583**, 711–719. https://doi.org/10.1038/s41586-020-2077-3 (2020).
14. Zhu, R. H. et al. The Mechanism of Insulin-Like Growth Factor II mRNA-Binging Protein 3 Induce Decidualization and Maternal-Fetal Interface Cross Talk by TGF-beta1 in Recurrent Spontaneous Abortion. *Front. Cell. Dev. Biol.* **10**, 862180. https://doi.org/10.3389/fcell.2022.862180 (2022).
15. Du, L. et al. Single-cell transcriptome analysis reveals defective decidua stromal niche attributes to recurrent spontaneous abortion. *Cell. Prolif.* **54**, e13125. https://doi.org/10.1111/cpr.13125 (2021).
16. Liu, X. et al. Comprehensive Analysis of circRNAs, miRNAs, and mRNAs Expression Profiles and ceRNA Networks in Decidua of Unexplained Recurrent Spontaneous Abortion. *Front. Genet.* **13**, 858641. https://doi.org/10.3389/fgene.2022.858641 (2022).
17. Butler, A., Hoffman, P., Smibert, P., Papalexi, E. & Satija, R. Integrating single-cell transcriptomic data across different conditions, technologies, and species. *Nat. Biotechnol.* **36**, 411–420. https://doi.org/10.1038/nbt.4096 (2018).
18. Kim, D., Langmead, B. & Salzberg, S. L. HISAT: a fast spliced aligner with low memory requirements. *Nat. Methods.* **12**, 357–360. https://doi.org/10.1038/nmeth.3317 (2015).
19. Trapnell, C. et al. Transcript assembly and quantification by RNA-Seq reveals unannotated transcripts and isoform switching during cell differentiation. *Nat. Biotechnol.* **28**, 511–515. https://doi.org/10.1038/nbt.1621 (2010).
20. Korsunsky, I. et al. Fast, sensitive and accurate integration of single-cell data with Harmony. *Nat. Methods.* **16**, 1289–1296. https://doi.org/10.1038/s41592-019-0619-0 (2019).
21. Ianevski, A., Giri, A. K. & Aittokallio, T. Fully-automated and ultra-fast cell-type identification using specific marker combinations from single-cell transcriptomic data. *Nat. Commun.* **13**, 1246. https://doi.org/10.1038/s41467-022-28803-w (2022).
22. Love, M. I., Huber, W. & Anders, S. Moderated estimation of fold change and dispersion for RNA-seq data with DESeq2. *Genome Biol.* **15**, 550. https://doi.org/10.1186/s13059-014-0550-8 (2014).
23. Qiu, X. et al. Reversed graph embedding resolves complex single-cell trajectories. *Nat. Methods.* **14**, 979–982. https://doi.org/10.1038/nmeth.4402 (2017).
24. Xie, C. et al. KOBAS 2.0: a web server for annotation and identification of enriched pathways and diseases. *Nucleic Acids Res.* **39**, W316–322. https://doi.org/10.1093/nar/gkr483 (2011).
25. Castello, A. et al. Insights into RNA biology from an atlas of mammalian mRNA-binding proteins. *Cell* **149**, 1393–1406. https://doi.org/10.1016/j.cell.2012.04.031 (2012).
26. Aibar, S. et al. SCENIC: single-cell regulatory network inference and clustering. *Nat. Methods.* **14**, 1083–1086. https://doi.org/10.1038/nmeth.4463 (2017).
27. Ritchie, M. E. et al. limma powers differential expression analyses for RNA-sequencing and microarray studies. *Nucleic Acids Res.* **43**, e47. https://doi.org/10.1093/nar/gkv007 (2015).
28. Suo, S. et al. Revealing the Critical Regulators of Cell Identity in the Mouse Cell Atlas. *Cell Rep* 25, 1436–1445 e1433, (2018). https://doi.org/10.1016/j.celrep.2018.10.045
29. Baltz, A. G. et al. The mRNA-bound proteome and its global occupancy profile on protein-coding transcripts. *Mol. Cell.* **46**, 674–690. https://doi.org/10.1016/j.molcel.2012.05.021 (2012).
30. Sun, Q. & Zhang, X. L. Research on apoptotic signaling pathways of recurrent spontaneous abortion caused by dysfunction of trophoblast infiltration. *Eur. Rev. Med. Pharmacol. Sci.* **21**, 12–19 (2017).
31. Gupta, S., Agarwal, A., Banerjee, J. & Alvarez, J. G. The role of oxidative stress in spontaneous abortion and recurrent pregnancy loss: a systematic review. *Obstet. Gynecol. Surv.* **62**, 335–347. https://doi.org/10.1097/01.ogx.0000261644.89300.df (2007). quiz 353 – 334.
32. RPL, E. G. G. et al. ESHRE guideline: recurrent pregnancy loss. *Hum Reprod Open* hoy004, (2018). https://doi.org/10.1093/hropen/hoy004 (2018).

33. Practice Committee of the American Society for Reproductive. Evaluation and treatment of recurrent pregnancy loss: a committee opinion. *Fertil. Steril.* **98**, 1103–1111. https://doi.org/10.1016/j.fertnstert.2012.06.048 (2012).
34. Salker, M. S. et al. Deregulation of the serum- and glucocorticoid-inducible kinase SGK1 in the endometrium causes reproductive failure. *Nat. Med.* **17**, 1509–1513. https://doi.org/10.1038/nm.2498 (2011).
35. Salker, M. S. et al. Disordered IL-33/ST2 activation in decidualizing stromal cells prolongs uterine receptivity in women with recurrent pregnancy loss. *PLoS One*. **7**, e52252. https://doi.org/10.1371/journal.pone.0052252 (2012).
36. Haig, D. Cooperation and conflict in human pregnancy. *Curr. Biol.* **29**, R455–R458. https://doi.org/10.1016/j.cub.2019.04.040 (2019).
37. Jin, B. et al. Deciphering decidual deficiencies in recurrent spontaneous abortion and the therapeutic potential of mesenchymal stem cells at single-cell resolution. *Stem Cell. Res. Ther.* **15**, 228. https://doi.org/10.1186/s13287-024-03854-6 (2024).
38. Zhang, H. et al. The roles of RNA-binding proteins in ovarian aging. *J. Assist. Reprod. Genet*. https://doi.org/10.1007/s10815-025-03765-2 (2025).
39. Wang, L. et al. Decorin promotes decidual M1-like macrophage polarization via mitochondrial dysfunction resulting in recurrent pregnancy loss. *Theranostics* **12**, 7216–7236. https://doi.org/10.7150/thno.78467 (2022).
40. Halari, C. D., Zheng, M. & Lala, P. K. Roles of Two Small Leucine-Rich Proteoglycans Decorin and Biglycan in Pregnancy and Pregnancy-Associated Diseases. *Int. J. Mol. Sci.* **22** https://doi.org/10.3390/ijms221910584 (2021).
41. Dumic, J., Dabelic, S. & Flogel, M. Galectin-3: an open-ended story. *Biochim. Biophys. Acta*. **1760**, 616–635. https://doi.org/10.1016/j.bbagen.2005.12.020 (2006).
42. Abramovic, I. et al. LGALS3 cfDNA methylation in seminal fluid as a novel prostate cancer biomarker outperforming PSA. *Prostate* **84**, 1128–1137. https://doi.org/10.1002/pros.24749 (2024).
43. Dong, R. et al. Galectin-3 as a novel biomarker for disease diagnosis and a target for therapy (Review). *Int. J. Mol. Med.* **41**, 599–614. https://doi.org/10.3892/ijmm.2017.3311 (2018).
44. Jovanovic Krivokuca, M. et al. Galectins in Early Pregnancy and Pregnancy-Associated Pathologies. *Int. J. Mol. Sci.* **23** https://doi.org/10.3390/ijms23010069 (2021).
45. Xiao, Q. et al. Expression of galectin-3 and apoptosis in placental villi from patients with missed abortion during early pregnancy. *Exp. Ther. Med.* **17**, 2623–2631. https://doi.org/10.3892/etm.2019.7227 (2019).
46. Fort, J. et al. The structure of human 4F2hc ectodomain provides a model for homodimerization and electrostatic interaction with plasma membrane. *J. Biol. Chem.* **282**, 31444–31452. https://doi.org/10.1074/jbc.M704524200 (2007).
47. Fotiadis, D., Kanai, Y. & Palacin, M. The SLC3 and SLC7 families of amino acid transporters. *Mol. Aspects Med.* **34**, 139–158. https://doi.org/10.1016/j.mam.2012.10.007 (2013).
48. Shi, J. W. et al. TNFSF14(+) natural killer cells prevent spontaneous abortion by restricting leucine-mediated decidual stromal cell senescence. *EMBO J.* **43**, 5018–5036. https://doi.org/10.1038/s44318-024-00220-3 (2024).
49. Khalaj, K. et al. RNA binding protein, tristetraprolin in a murine model of recurrent pregnancy loss. *Oncotarget* **7**, 72486–72502. https://doi.org/10.18632/oncotarget.12539 (2016).
50. Dai, F. et al. IGF2BP3 participates in the pathogenesis of recurrent spontaneous abortion by regulating ferroptosis. *J. Reprod. Immunol.* **165**, 104271. https://doi.org/10.1016/j.jri.2024.104271 (2024).
51. Zhang, W. et al. Deciphering the IGF2BP3-mediated control of ferroptosis: mechanistic insights and therapeutic prospects. *Discov Oncol.* **15**, 547. https://doi.org/10.1007/s12672-024-01432-z (2024).

Author contributions

Q.Y. were responsible for study concept and design. Y.Z. was in charge of drafting the manuscript. Y.Z., X.W and A.L. performed data analysis. Q.Y. B.X. and D.C. contributed to critical revision of the manuscript for important intellectual contents. All authors have read and agreed to the published version of the manuscript.

Funding

No funding was received.

Declarations

Competing interest

The authors declare no competing interests.

Additional information

Supplementary Information The online version contains supplementary material available at https://doi.org/10.1038/s41598-026-45052-9.

Correspondence and requests for materials should be addressed to Q.Y.

Reprints and permissions information is available at www.nature.com/reprints.

Publisher's note Springer Nature remains neutral with regard to jurisdictional claims in published maps and institutional affiliations.